

See discussions, stats, and author profiles for this publication at: <https://www.researchgate.net/publication/224283152>

Aerosol-Based Fabrication of Biocompatible Organic-Inorganic Nanocomposites

ARTICLE *in* ACS APPLIED MATERIALS & INTERFACES · MAY 2012

Impact Factor: 6.72 · DOI: 10.1021/am300337c · Source: PubMed

CITATIONS

17

READS

59

2 AUTHORS:



[Jeong Hoon Byeon](#)

Yeungnam University

89 PUBLICATIONS 997 CITATIONS

[SEE PROFILE](#)



[Jeffrey Roberts](#)

Purdue University

113 PUBLICATIONS 1,988 CITATIONS

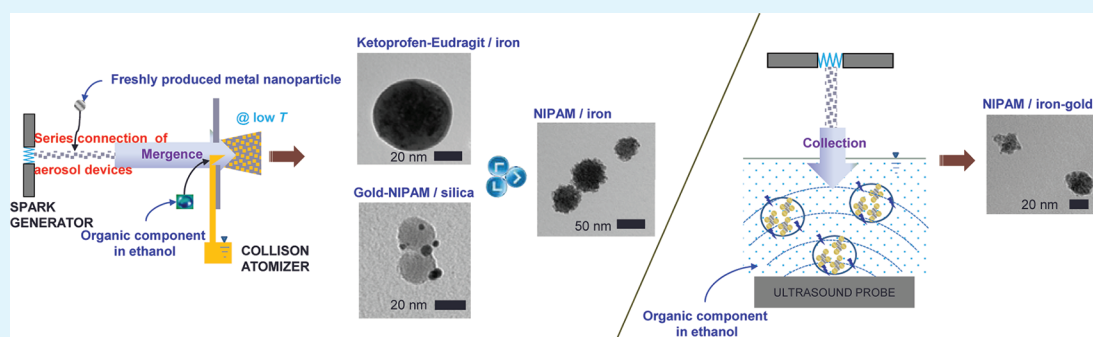
[SEE PROFILE](#)

Aerosol-Based Fabrication of Biocompatible Organic–Inorganic Nanocomposites

Jeong Hoon Byeon and Jeffrey T. Roberts*

Department of Chemistry, Purdue University, Indiana 47907, United States

Supporting Information



ABSTRACT: Several novel nanoparticle composites were conveniently obtained by appropriately reacting freshly produced aerosol metal nanoparticles with soluble organic components. A serial reactor consisting of a spark particle generator coupled to a collision atomizer was used to fabricate the new materials, which included nanomagnetosols (comprising iron nanoparticles, the drug ketoprofen, and a Eudragit shell), hybrid nanogels (comprising iron nanoparticles and an *N*-isopropylacrylamide, NIPAM, gel), and nanoinorganics (gold immobilized silica). A fourth hybrid material, consisting of iron–gold nanoparticles and NIPAM) was obtained via an aerosol into liquid configuration, in which aerosol iron–gold particles were collected into a NIPAM/ethanol solution and then formed into nanogels with NIPAM under ultrasonic treatment. The strategy outlined in this work is potentially generalizable as a new platform for creating biocompatible nanocomposites, using only clinically approved starting materials in a single pass and under low-temperature conditions.

KEYWORDS: *novel nanocomposites, nanomanetosols, hybrid nanogels, nanoinorganics*

Many novel nanomaterials have recently been developed for potential biomedical applications, each with advantages and disadvantages in terms of biocompatibility, bioavailability, pharmacokinetics, immunogenicity, and toxicity. Most syntheses are still conducted using time-consuming batch processes, increasing expense and limiting the ability to control or install desired functionalities. In contrast to classical wet chemical methods, aerosol processing involves a much more limited number of preparation steps. It also produces material continuously, allows for straightforward collection of particles and generates low waste.¹ The combination of aerosol processing and more conventional chemical routes has the potential to bring a “wind of change” to the synthesis of advanced nanomaterials.² This strategy may give birth to a promising family of innovative nanomaterials with many desirable applications, both realized and potential, in biomedical domains, such as functional coatings, biomaterials, multifunctional therapeutic carriers, and controlled release.³ The field of therapeutic aerosol bioengineering, driven originally primarily by the medical need for inhaled insulin, is now expanding to address medical needs ranging from respiratory to systemic diseases.⁴

Although potential biomedical applications of conventional aerosol methods have been studied in detail,^{5–7} mostly in the

pharmaceutical industry to generate spherical microparticles, their potential has received comparatively little attention in nanobiomedicine. Nevertheless, aerosol processes have shown potential as a route to hybrid micro/nano nanomaterials for use in magnetic resonance imaging, hyperthermia, and controlled/targeted drug delivery.^{8–15} From a processing point of view, an aerosol synthesis reactor typically consists of two or three heating zones to dry (at ~200 °C) liquid droplets (starting materials) and to calcine/sinter (at 500–1500 °C) particles.^{16,17} Such high temperatures can induce decomposition of organic components (i.e., biocompatible nanomaterials). For this reason, the aerosol equivalent of a one-pot approach^{18,19} is not viable for synthesizing biocompatible nanomaterials without expensive and time-consuming postfunctionalization strategies.² An important nanotechnological challenge can be addressed via the tuning of hybrid organic–inorganic interfaces in nanobiomedicine field. Clearly, a method is needed that operates entirely at low processing temperatures, thereby

Received: February 24, 2012

Accepted: April 17, 2012

Published: April 17, 2012



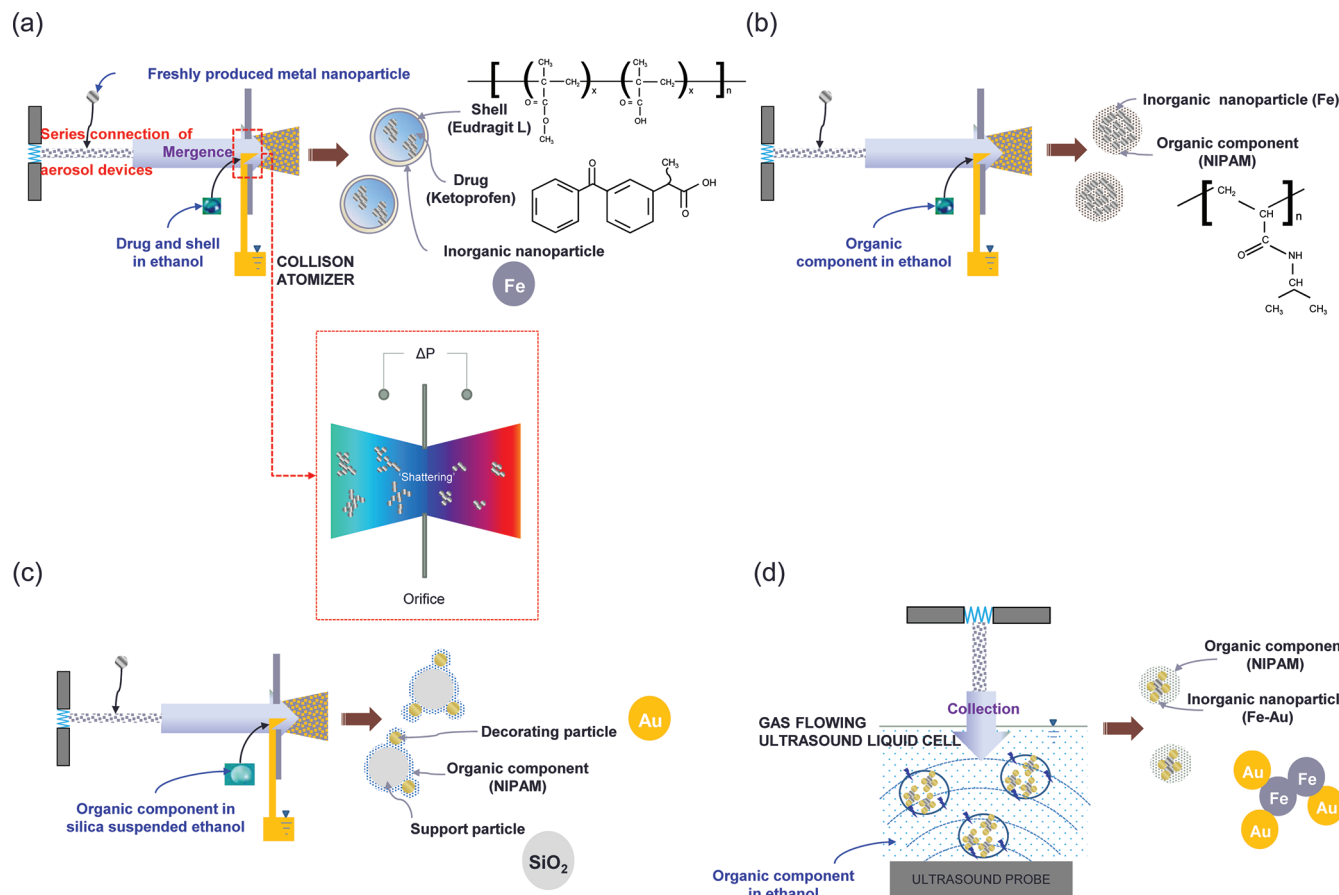


Figure 1. Reactors used to fabricate: (a) nanomagnetosols, (b, d) hybrid nanogels, and (c) nanoinorganics. a–c show series connections of spark generator and a collision atomizer. d shows a series reactor of a spark generator coupled to ultrasound probe inserted into a gas flow liquid cell.

allowing introduction of heat-sensitive organic molecules into an inorganic network at the nanometer scale.²⁰

In this work, we present a simple aerosol-based method in which organic and inorganic components are combined to fabricate nanomagnetosols (comprising iron nanoparticles, the drug ketoprofen, and Eudragit shells), hybrid nanogels (comprising iron nanoparticles and *N*-isopropylacrylamide, NIPAM, gel), and nanoinorganics (gold immobilized silica). Syntheses are performed in a serial aerosol reactor developed by Byeon and Roberts (BR) which allows freshly produced aerosol metal nanoparticles to be embedded into organic matrices “on the fly” by merging them appropriately in a one-pass ambient gas stream. The merged particles are then thermally treated at low temperatures (<40 °C) to extract only the accompanying solvent, with no further high temperature treatments. In an elaboration of this strategy, hybrid nanogels are also fabricated using an “aerosol into liquid” configuration consisting of an aerosol device and a gas flow ultrasound liquid cell.

METHODS

Schematic diagrams of the reactors used for these experiments are shown in Figure 1a–d. Briefly, a spark generator produces aerosol metal nanoparticles (iron, gold, or iron–gold). Spark generation has been used to produce a variety of metallic, carbonaceous, and other composite materials with nanoscale dimensions at ambient temperatures and pressures.^{21–25} The specifications of the discharge configuration were as follows: electrode diameter and length, 3 mm and 100 mm, respectively; resistance, 0.5 MΩ; capacitance, 1.0 nF; loading current, 1.8–3.0 mA; applied voltage, 2.6–3.4 kV; and

frequency, 540–800 Hz. To fabricate model nanomagnetosols (comprised of magnetically responsive nanoparticles along with a drug of choice),^{26,27} an iron nanoparticle-laden nitrogen (>99.99% purity) flow (2 L min^{−1}) was used as the operating gas for atomizing a solution containing ketoprofen [2-(3-benzoylphenyl) propionic acid, Sigma, US] and Eudragit (L 100 PO, acrylic polymer, Röhm Pharma, Germany) dissolved in ethanol (99.5%, EMD Millipore, US), (Figure 1a). The iron nanoparticles passed over the atomizer orifice, where they mixed with atomized particles to form hybrid droplets. The droplets then pass through a heated tubular flow reactor operating at 60 °C wall temperature to drive ethanol from the droplets (refer to the Supporting Information). The resulting particles were diluted (dilution ratio = 5) with nitrogen gas to prevent agglomeration. Other nanohybrids described in this work were grown using modifications of this apparatus (see Figure 1b, c), but with different cathode-anode spark configurations and different solutions: iron–iron/NIPAM (99.0% Acros Organics, US) in ethanol for Figure 1b, and iron–gold/NIPAM in silica (20 nm in diameter, M K Impex, Canada) suspended ethanol for Figure 1c. To verify the feasibility of the “aerosol into liquid” configuration, we injected iron–gold nanoparticles (from an iron–gold spark discharge) laden gas into an ultrasound probe inserted liquid (NIPAM/ethanol) cell (Figure 1d). The total solid concentrations of the solutions are fixed at 1.4 g L^{−1} for all configurations.

RESULTS AND DISCUSSION

Figure 2a summarizes results for the nanomagnetosol synthesis. The total number concentration (TNC), geometric mean diameter (GMD), and geometric standard deviation (GSD) of the merged particles are 4.08×10^6 particles cm^{−3}, 38.7 nm, and 1.69, respectively. The same measurements for individual

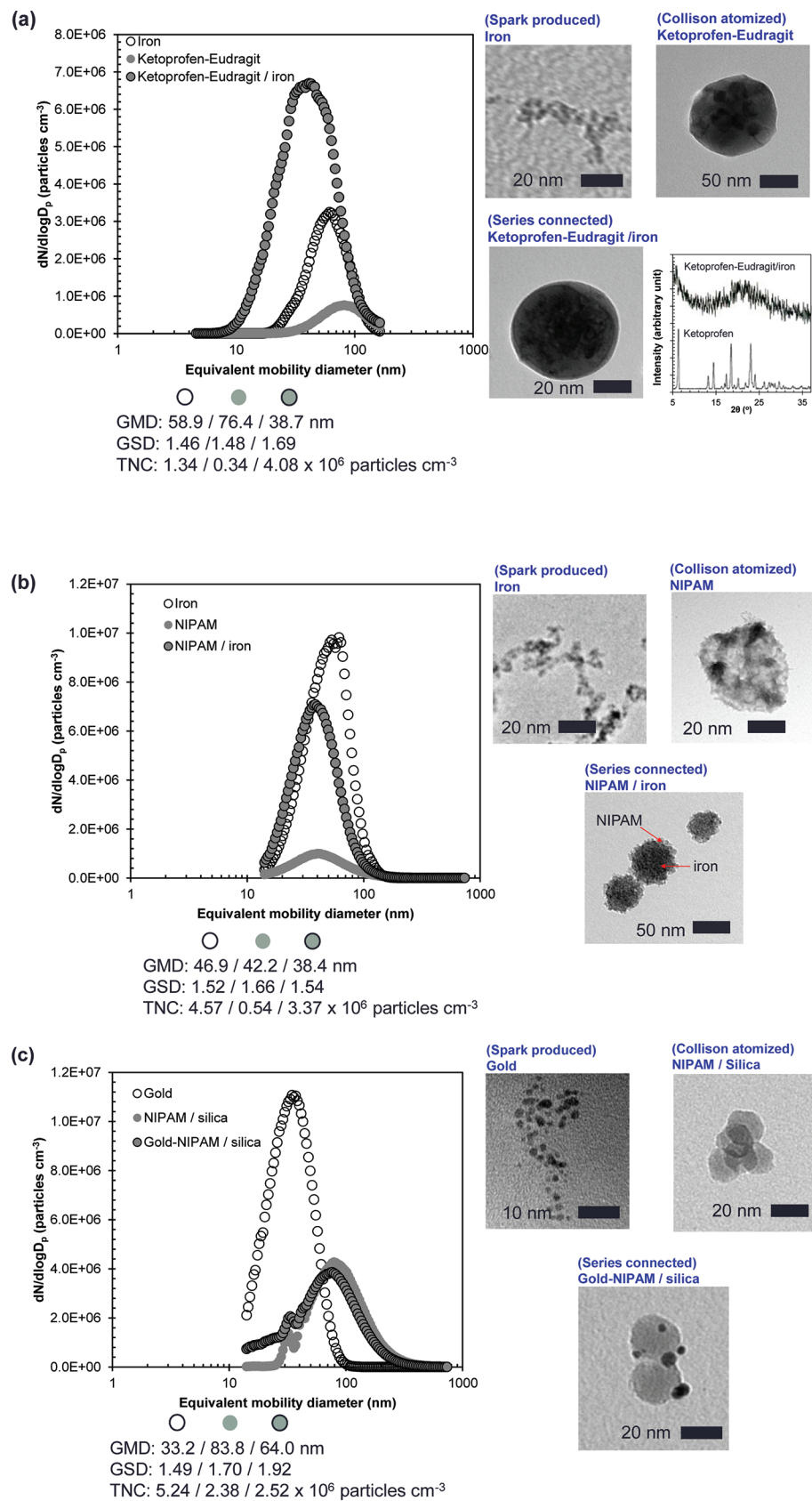


Figure 2. continued

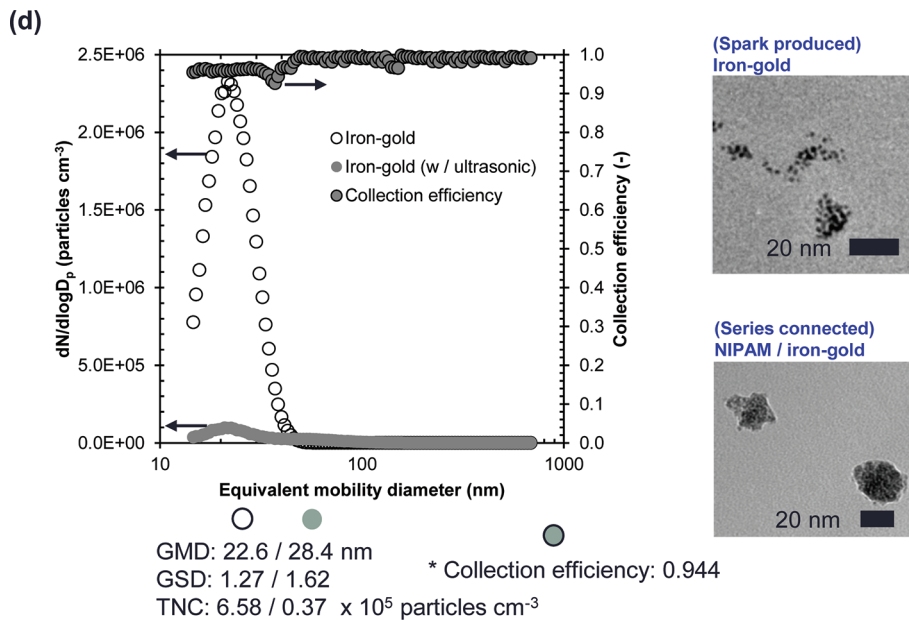


Figure 2. Characterization of four new nanoparticle composites: (a) size distributions, TEM micrographs, and X-ray diffraction patterns of ketoprofen and nanomagnetosols; (b) size distributions and TEM micrographs of hybrid nanogels (iron, NIPAM, and NIPAM/iron); (c) size distributions and TEM micrographs of nanoinorganics (gold, NIPAM/silica, and gold-NIPAM/silica); (d) size distributions of iron–gold with and without ultrasound, the corresponding collection efficiency of iron–gold into NIPAM/ethanol solution, and TEM micrographs of iron–gold and NIPAM/iron–gold.

iron particles are 1.34×10^6 particles cm^{-3} , 58.9 nm, 1.46, respectively, and for ketoprofen-Eudragit droplet particles they are 0.34×10^6 particles cm^{-3} , 76.4 nm, and 1.48, respectively. A replacement of the size distribution after merging iron nanoparticles with ketoprofen-Eudragit droplets is represented by deagglomeration (by setting the force acting on an agglomerate of size D_{pa} due to the sudden pressure change across an orifice in the collision atomizer), and is given by²⁸

$$D_p = \alpha \sqrt{\frac{D_{pa}H}{6\pi\Delta P\Theta^2}} \quad (1)$$

where D_p is the size of a restructured agglomerate, α is the proportionality constant, H is the Hamaker constant, ΔP is the pressure difference between the front and the rear of an orifice, and Θ is the parameter controlling the maximum cohesive strength between constituting particles in an agglomerate. Iron agglomerates pass through the orifice, and the rapid changes in pressure, density, and velocity across the orifice produce an impulse capable of shattering the agglomerates (refer to the dotted area in Figure 1a). Figure 2a shows typical transmission electron microscope (TEM) micrographs of the spark produced iron, collision atomized ketoprofen-Eudragit, and their merged nanostructures. The spark produced iron nanoparticles are agglomerated compared to ketoprofen-Eudragit spherical particles. The spherical particles have smooth surfaces, and show no crystallites. Free iron particles have a tendency to agglomerate to reduce surface energy, regardless of magnetic properties. When particles are encapsulated with surfactant and polymer, agglomeration is reduced,²⁹ affording the attainment of size distributions like that shown in Figure 2a. The dark contrast in the bottom micrograph can be assigned as iron from energy dispersive X-ray (JED-2200, JEOL, Japan) analyses, and the size reduced iron agglomerates which are confined inside the spherical matrix. Figure 2a shows powder X-ray diffractograms of ketoprofen and nanomagnetosol (ketoprofen amount: 30%, *w/w*) samples. The pure ketoprofen samples shows sharp peaks demonstrating the crystalline nature of the drug, whereas the nanomagnetosol sample shows broad and diffuse peaks, indicating poor crystallinity. Some weak diffraction features of crystalline ketoprofen can be identified in the diffractograms of nanomagnetosol at $2\theta \approx 6$ and 23° .^{30,31} The diffuse and weak nature of the peaks is consistent with dispersion of the drug throughout the matrix.

Figure 2b shows the results of fabricated hybrid nanogels (iron nanoparticles as the cross-linker and NIPAM as the monomer without a chemical cross-linker), which contains particle size distributions and TEM micrographs of iron, NIPAM, and their merged nanostructures. The size distribution of the nanogels is different from those of pure iron or NIPAM particles, as was observed for the nanomagnetosol particles. The merged particles in this case are smaller than the pure NIPAM particles. This size reduction is characterized by the parameter β in eq 2, where, $V_p(T)$ (or $R_p(T)$) and V_{p0} (or R_{p0}) are the NIPAM volumes (or radii) of particles at temperature T and in the fully swollen state, respectively.³² The bushy extended structures that characterize the reactant iron particles have vanished, to be replaced by looplike nanogels (see Figure 2b), where shattered iron particles are locked inside the looplike network. The cross-linking points are probably formed *via* natural electrostatic charges³³ and/or interparticle termination of propagating radicals on the iron particles,³⁴ because there are no added chemical cross-linkers.

$$\beta = \frac{V_p(T)}{V_{p0}} = \left(\frac{R_p(T)}{R_{p0}} \right)^3 \quad (2)$$

A previous study reported that inorganic nanoparticles embedded inside NIPAM collapsed in structure above the lower critical solution temperature (32°C), i.e., in the presence of hydrophobic NIPAM.³⁵ This induces a decrease of the fractal

dimension of iron particles in the nanogel, and thus the number of agglomerates N after merging is smaller than it would be for individual iron particles (see eq 3, where k_g is the fractal prefactor, D_{p0} is the size of a primary iron particle, and d_f is the fractal dimension), distinguished by the nanomagnetosol case.

$$N = k_g \left(\frac{D_p}{D_{p0}} \right)^{d_f} \quad (3)$$

These interesting results may suggest a highly flexible approach to hybrid nanogels with inorganic nanoparticles with respect to preparation without the use of a chemical cross-linker, since not only the organic composition and the inorganic nanoparticle materials, size, and shape, but also the morphology of the overall hybrid system, can be varied.

Gold decorated silica nanoparticles as nanoinorganics are also easily fabricated via the BR method (Figure 2c). The gold particles are nearly quantitatively incorporated into silica, to form a new composite material. The size distribution of merged particles is nearly same as for NIPAM, which in this case serves as a binder between gold and silica. This is due to coagulation (heterogeneous) of gold and silica before the coagulation (homogeneous) of gold at the position around the orifice in a Collison atomizer. Equation 4 describes the decrease in the number concentration of gold nanoparticles as a function of collisions within the gold as well as collisions with silica, where the concentration is consistent:

$$\frac{dC_{\text{gold}}}{dt} \propto (K_{\text{gold}} C_{\text{gold}}^2 + K_{\text{silica}} C_{\text{gold}} C_{\text{silica}}) \quad (4)$$

where C_{gold} and C_{silica} are the respective number concentrations of gold and silica particles, K_{gold} ($=((4kT)/(3\mu))$) and K_{silica} ($=((2kT d_{\text{gold}})/(3\mu d_{\text{silica}}))$) are the respective collision frequency functions for homogeneous and heterogeneous collisions (where k is the Boltzmann factor, T is the temperature, and μ the gas viscosity). Correspondingly, in TEM micrographs (Figure 2c), gold/NIPAM/silica show deagglomerated gold and the attached gold particles being smaller and more narrowly dispersed than were the individual gold particles. Nanoinorganics, such as gold and silica, already have received much attention as new drug delivery and diagnostic agents.^{36,37} Considering these applications, the results are a promising good platform to fabricate multifunctional nanoinorganics for use in future biomedical applications. Moreover, typical silica decoration with gold is costly and time-consuming, and high temperature calcination ($>500\text{ }^\circ\text{C}$) is required.^{38,39}

Figure 2d shows a fourth hybrid nanogel, fabricated using the “aerosol into liquid” system. We used an iron–gold spark configuration, because the bimetallic nanoparticles are of special interest since gold provides a useful surface chemistry and biological reactivity.⁴⁰ In this system, effective collection of the aerosol nanoparticles into a NIPAM/ethanol solution cell is the most critical aspect of the process. Previous studies have been shown low efficiencies (<40%) of collection of aerosol particles injected into liquid.^{41,42} To circumvent this problem, low-frequency ultrasound (20 kHz) was applied to the liquid to enhance the collection and reactivity between iron–gold and NIPAM components. The fractional (grade) collection efficiency of the cell ($\eta_{\text{ultrasonic}}$) is defined by

$$\eta_{\text{ultrasonic}}(D_p) = 1 - \frac{C(D_p)}{C_0(D_p)} \quad (5)$$

where $C(D_p)$ is the number concentration of particles with size D_p measured at the gas exit of the cell when the ultrasound is applied to the solution. The iron–gold (20 nm in mean equivalent mobility diameter) is nearly quantitatively transferred to solution (~94%, shown in Figure 2d) by the enhancement of particle velocity in the presence of ultrasound (accelerated velocity, $\sim 250\text{ m s}^{-1}$).⁴³ Therefore, nanogels similar to those in Figure 2b were also successfully fabricated by this configuration.

The production yields of nanomagnetosols, hybrid nanogels, nanoinorganics, and hybrid nanogels from aerosol-liquid method are approximately 79, 73, 85, and 86%, respectively. Yields were determined by the area fraction of nanocomposites-to-all particles in the TEM image. Furthermore, the cytotoxicity of the nanocomposite/plasmid DNA complexes is evaluated by MTS, 3-(4,5-dimethyl-thiazol-2-yl)-5-(3-carboxymethoxyphenyl)-2-(4-sulfophenyl)2H-tetrazolium, assay in human embryonic kidney 293 cells, with different storage days (Table 1).

Table 1. Cytotoxicity of Synthesized Nanocomposites (tested after synthesized 5, 30, and 90 days)

case	cell viability (%)		
	5 days	30 days	90 days
nanomagnetosols	88.6	89.1	86.9
hybrid nanogels	79.8	79.7	79.4
nanoinorganics	83.0	81.9	82.6
hybrid nanogels (aerosol-liquid)	80.1	80.5	79.8

The results show that the range of cell viability is about 80%–90% for all the tested nanocomposites, and there are no significant differences between the storage days. This implies that the nanocomposites have biocompatibility and stability that may be suitable in a clinical context.

CONCLUSIONS

For the first time, an aerosol-based method has been used to aerosol construct biocompatible nanocomposites composed of organic and inorganic components. This method can generate biocompatible nanocomposites from only clinically approved starting materials in a single pass and under low temperature conditions. Similar aerosol-based strategies may allow the extension for fabricating other biocompatible nanocomposites. In future work, these strategies will be demonstrated for their possibilities in the field of biomedical applications.

ASSOCIATED CONTENT

Supporting Information

The instrumental details, temperature profile in a heated tubular reactor, magnetization of ketoprofen-Eudragit/iron, NIPAM/iron, and NIPAM/gold–iron at 293 K, and aerosol magnetic sampling of ketoprofen-Eudragit/iron particles. This material is available free of charge via the Internet at <http://pubs.acs.org/>.

AUTHOR INFORMATION

Corresponding Author

*Address: Purdue University Mathematical Sciences Building, 150 N. University Street, West Lafayette, Indiana 47907-2067, United States. E-mail: jtrob@purdue.edu. Tel: (+1-765) 494-1730. Fax: (+1-765) 494-1736.

Notes

The authors declare no competing financial interest.

ACKNOWLEDGMENTS

This work was partially supported by NSF Grant CHE-0924431.

REFERENCES

- (1) Pratsinis, S. E. *AIChE J.* **2010**, *56*, 3028.
- (2) Boissiere, C.; Grosso, D.; Chaumonnot, A.; Nicole, L.; Sanchez, C. *Adv. Mater.* **2011**, *23*, 599.
- (3) Yang, W.; Peters, J. I.; Williams, R. O., III. *Int. J. Pharm.* **2008**, *356*, 239.
- (4) Edwards, D. A.; Dunbar, C. *Annu. Rev. Biomed. Eng.* **2002**, *4*, 93.
- (5) Dolovich, M. B.; Dhand, R. *Lancet* **2011**, *377*, 1032.
- (6) Okuyama, K.; Abdullah, M.; Lenggoro, I. W.; Iskandar, F. *Adv. Powder Technol.* **2006**, *17*, 587.
- (7) Iskandar, F.; Lenggoro, I. W.; Xia, B.; Okuyama, K. *J. Nanopart. Res.* **2001**, *3*, 263.
- (8) Julián-López, B.; Boissière, C.; Chanéac, C.; Grosso, D.; Vasseur, D.; Miraux, S.; Duguet, E.; Sanchez, C. *J. Mater. Chem.* **2007**, *17*, 1563.
- (9) Buranda, T.; Huang, J.; Ramarao, G. V.; Ista, L. K.; Larson, R. S.; Ward, T. L.; Sklar, L. A.; Lopez, G. P. *Langmuir* **2003**, *19*, 1654.
- (10) Ruiz-Hernández, E.; López-Noriega, A.; Arcos, D.; Izquierdo-Barba, I.; Terasaki, O.; Vallet-Regí, M. *Chem. Mater.* **2007**, *19*, 3455.
- (11) Arcos, D.; López-Noriega, A.; Arcos, D.; Ruiz-Hernández, E.; Terasaki, O.; Vallet-Regí, M. *Chem. Mater.* **2009**, *21*, 1000.
- (12) Colilla, M.; Manzano, M.; Izquierdo-Barba, I.; Vallet-Regí, M.; Boissière, C.; Sanchez, C. *Chem. Mater.* **2010**, *22*, 1821.
- (13) Liu, J.; Jiang, X.; Ashley, C.; Brinker, C. J. *J. Am. Chem. Soc.* **2009**, *131*, 7567.
- (14) Ruiz-Hernández, E.; López-Noriega, A.; Arcos, D.; Vallet-Regí, M. *Solid State Sci.* **2008**, *10*, 421.
- (15) Liu, J.; Stace-Naughton, A.; Jiang, X.; Brinker, C. J. *J. Am. Chem. Soc.* **2009**, *131*, 1354.
- (16) Nandyanto, A. B. D.; Hagura, N.; Iskandar, F.; Okuyama, K. *Acta Mater.* **2010**, *58*, 282.
- (17) Iskandar, F.; Mikrajuddin; Okuyama, K. *Nano Lett.* **2002**, *2*, 389.
- (18) Sanchez, C.; Boissiere, C.; Grosso, D.; Laberty, C.; Nicole, L. *Chem. Mater.* **2008**, *20*, 682.
- (19) Nicole, L.; Boissière, C.; Grosso, D.; Quach, A.; Sanchez, C. J. *Mater. Chem.* **2005**, *15*, 3598.
- (20) Sanchez, C.; Soler-illia, G. J.; de, A. A.; Ribot, F.; Lalot, T.; Mayer, C. R.; Cabuil, V. *Chem. Mater.* **2001**, *13*, 3061.
- (21) Byeon, J. H.; Park, J. H.; Hwang, J. *J. Aerosol Sci.* **2008**, *39*, 888.
- (22) Byeon, J. H.; Park, J. H.; Yoon, K. Y.; Ko, B. J.; Ji, J. H.; Hwang, J. *Carbon* **2006**, *44*, 2106.
- (23) Byeon, J. H.; Park, J. H.; Yoon, K. Y.; Hwang, J. *Nanoscale* **2009**, *1*, 339.
- (24) Byeon, J. H.; Kim, J. -W. *Appl. Phys. Lett.* **2010**, *96*, 153102.
- (25) Byeon, J. H.; Kim, J. -W. *ACS Appl. Mater. Interfaces* **2010**, *2*, 947.
- (26) Dames, P.; Gleich, B.; Flemmer, A.; Hajek, K.; Seidl, N.; Wiekhorst, F.; Eberbeck, D.; Bittmann, I.; Bergemann, C.; Weyh, T.; Trahms, L.; Rosenecker, J.; Rudolph, C. *Nat. Nanotechnol.* **2007**, *2*, 495.
- (27) Plank, C. *Trends Biotechnol.* **2008**, *26*, 59.
- (28) To, D.; Dave, R.; Yin, X.; Sundaresan, S. *AIChE J.* **2009**, *55*, 2807.
- (29) Kayal, S.; Ramanujan, R. V. *J. Nanosci. Nanotechnol.* **2010**, *10*, 5527.
- (30) Eerikäinen, H.; Kauppinen, E. I.; Kansikas, J. *Pharm. Res.* **2004**, *21*, 136.
- (31) Manna, L.; Banchero, M.; Sola, D.; Ferri, A.; Ronchetti, S.; Sicardi, S. *J. Supercrit. Fluids* **2007**, *42*, 378.
- (32) Karg, M.; Hellweg, T. *Curr. Opin. Colloid Interface Sci.* **2009**, *14*, 438.
- (33) Byeon, J. H.; Kim, J. -W. *Langmuir* **2010**, *26*, 11928.
- (34) Czaun, M.; Hevesi, L.; Takafuji, M.; Ihara, H. *Chem. Commun.* **2008**, *18*, 2124.
- (35) Murugadoss, A.; Khan, A.; Chattopadhyay, A. *J. Nanopart. Res.* **2010**, *12*, 1331.
- (36) Chen, W.; Xu, N.; Wang, L.; Li, Z.; Ma, W.; Zhu, Y.; Xu, C.; Kotov, N. A. *Macromol. Rapid Commun.* **2010**, *31*, 228.
- (37) Weissleder, R. *Nat. Biotechnol.* **2001**, *19*, 316.
- (38) Phonthammachai, N.; White, T. J. *Langmuir* **2007**, *23*, 11421.
- (39) Kim, T. -H.; Kim, D. -W.; Lee, J. -M.; Lee, Y. -G.; Oh, S. -G. *Mater. Res. Bull.* **2008**, *43*, 1126.
- (40) Daniel, M. -C.; Astruc, D. *Chem. Rev.* **2004**, *104*, 293.
- (41) Miljevic, B.; Modini, R. L.; Bottle, S. E.; Ristovski, Z. D. *Atmos. Environ.* **2009**, *43*, 1372.
- (42) Dart, A.; Thornburg, J. *Atmos. Environ.* **2008**, *42*, 828.
- (43) Byeon, J. H.; Kim, Y. -W. *Ultrason. Sonochem.* **2012**, *19*, 209.